Enhanced neutral depletion in a static helium helicon discharge

2012 Plasma Sources Sci. Technol. 21 035008

(http://iopscience.iop.org/0963-0252/21/3/035008)

Plasma Sources Sci. Technol. **21** (2012) 035008 (8pp) doi:10.1088/0963-0252/21/3/035008

Enhanced neutral depletion in a static helium helicon discharge

Saeid Houshmandyar and Earl E Scime

Department of Physics, West Virginia University, Morgantown, WV 26506-6315, USA

Received 13 July 2011, in final form 24 April 2012
Published 23 May 2012
Online at stacks.iop.org/PSST/21/035008

Abstract
Laser-induced fluorescence (LIF) measurements of plasma opacity are used as a novel diagnostic to determine the absolute density of a metastable state of neutral helium atoms in a helicon plasma. The absorption scale length at a wavelength of 587.725 nm (vacuum) is determined from measurements of fluorescence intensity as a function of distance along the laser path. With a collisional–radiative model of the state populations, the absolute ground state neutral helium density is estimated from the metastable state density measurement. This paper expands upon previous work through measurements of neutral density, temperature and flow at different radial positions. The measured neutral density decreases by two orders of magnitude from the edge of the plasma to the axis of the plasma source. When the helicon source is operated in a static mode (i.e. no active gas pumping) the on-axis neutral density decreases by 69% from the pumping case and the on-axis plasma density increases by 42%; yielding an ionization fraction of approximately 90%.

(Some figures may appear in colour only in the online journal)

1. Introduction

Ion–neutral and electron–neutral collisions in low-temperature laboratory plasmas play critical roles in a variety of plasma phenomena. Neutral collisions damp waves, increase transport, and perhaps even impart momentum to ions and dust. In a plasma with an inhomogeneous neutral density profile, plasma rotation in the reverse $E \times B$ direction was attributed to collision-mediated ion–neutral momentum transfer [1]. In another partially ionized plasma, wave dispersion was measurably altered by collisions between neutrals and ions and electrons [2, 3]. In the core region of a high-density helicon source ($n \sim 10^{13}\,\mathrm{cm}^{-3}$), which is suitable for Alfvén wave studies at practical parallel length scales ($L \sim 2\,\mathrm{m}$), finite ion–neutral collisions can shift the ion-cyclotron resonance feature toward lower frequencies [4]. Although the high neutral pressures that yield high plasma densities are necessary for reducing the Alfvén wavelength to practical sizes in helicon sources, the resultant large neutral collision frequencies introduce additional complications. However, if in the core region of the helicon plasma the neutral density decreases significantly (a hollow neutral density profile), high plasma densities are achievable without the deleterious effects of large neutral collision frequencies.

Because of the importance of its effects on a variety of experiments, neutral depletion, i.e. neutral pumping has been the subject of a number of studies in helicon sources. An inductively coupled plasma (ICP) source operating in the high-density, 'helicon' mode (with a bright and distinctive core) can range from weakly ionized at the edge to nearly fully ionized in the center [5]. One of the first studies of neutral depletion in a helicon source involved the insertion of perturbing drift tubes into the discharge. The other end of the open drift tube was connected to a fast ion gauge and as the open tube end was moved across the plasma column, the gas pressure profile was measured [6]. Some groups have used spectroscopic techniques, such as emission line measurements coupled with collisional–radiative (CR) modeling [7] or two-photon laser-induced fluorescence (LIF) [8] to measure inhomogeneities in neutral density profiles arising from radially varying levels of electron-impact ionization and other effects, such as those introduced by magnetic nozzle geometries [9]. Other groups have assumed a uniform neutral pressure profile and employed spectroscopic measurements of the neutral temperature to infer that the neutral density decreases significantly along the axis of cylindrically symmetric low-temperature laboratory plasmas [10]. Theoretical studies [11–14] and computational modeling [15–17] often play key roles in studies of neutral depletion in laboratory plasma sources. Understanding and controlling the

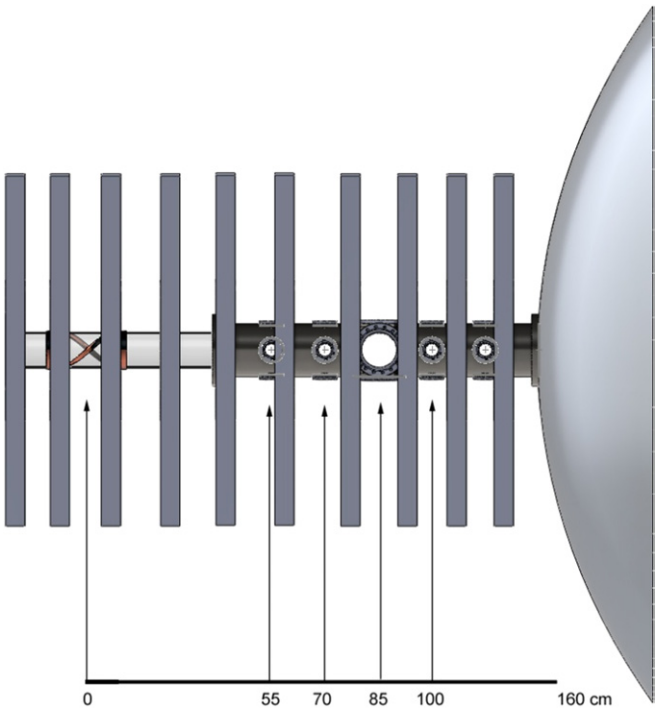

Figure 1. Schematic of the HELIX-LEIA apparatus (a portion of the end of the LEIA chamber is shown at the right of this figure). The 19 cm long $m = 1$ antenna surrounds the glass portion of the chamber at $z = 0$ cm. Ten electromagnets, aligned as shown, provide the magnetic field in the source region. The parallel laser injection optic was placed at $z = -100$ cm. Fluorescent emission was collected at distances of 55, 70, 85 and 100 cm downstream of the rf antenna.

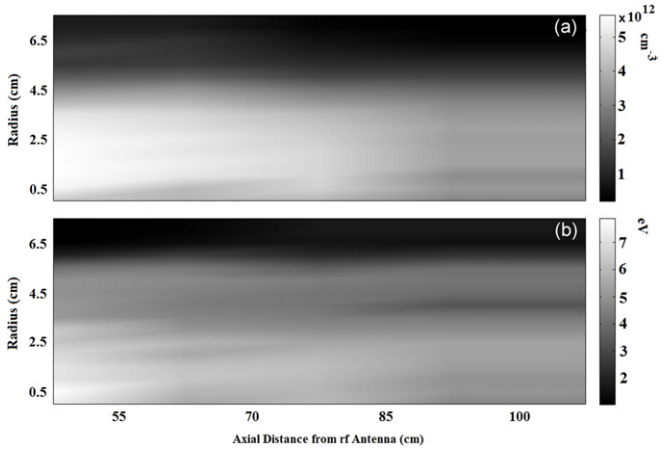

Figure 2. Smoothed plots of the measured (a) electron density and (b) electron temperature versus radial location and distance from rf antenna.

neutral profile in plasma sources is required to mitigate the deleterious effects of non-uniform neutral profiles, e.g. non-uniform etching in ICPs [18].

Recently, we developed a new approach to measuring the neutral helium density in helicon plasmas. The technique is based on LIF measurements of the optical depth of the plasma at a wavelength of 587.725 nm (in vacuum) [19]. In this work, we describe the application of that technique to measurements of the neutral density profile in a helicon source using a more powerful laser source. Based on the neutral density profile measurements, we also present evidence that static helicon discharges (no active gas pumping) lead to significantly reduced neutral densities and increased plasma densities along the source axis.

2. Experimental apparatus

The experiments reported in this paper were carried out in HELIX (Hot hELIcon eXperiment) at West Virginia University. HELIX is a traditional helicon plasma source and primarily designed for space-relevant laboratory experiments [20]. It has a hybrid stainless steel-Pyrex™ vacuum chamber: the Pyrex™ section is 61 cm long and 10 cm in diameter and is connected to the stainless steel section which is 91 cm long and 15 cm in diameter. Figure 1 shows a side view of the HELIX-LEIA system. The stainless steel section has one set of four 6 inch Conflat™ crossing ports in the center and four sets of four $2\frac{3}{4}$ inch Conflat™ crossing ports along the sides for diagnostic access. The stainless steel chamber opens into a 1.8 m diameter, 4.4 m long diffusion chamber, LEIA (Large Experiment on Instabilities and Anisotropies). A steady-state, axial magnetic field of 0–1400 G is maintained with ten water-cooled electromagnets. A 19 cm, half wavelength, right handed helical antenna is wrapped around the Pyrex™ section of the HELIX and couples rf power supplied from an ENI 1000 amplifier into the plasma. Up to 2 kW of rf power, over a frequency range 6–18 MHz, is used to generate the plasma. A capacitive π circuit impedance matches the antenna to the rf amplifier. A base pressure of 10^{-8} Torr is maintained in the HELIX-LEIA system with three turbomolecular drag pumps (two 1600 L s^{-1} pumps at the LEIA end of the chamber and one 540 L s^{-1} at the HELIX end of the chamber). An MKS 1179 mass flow valve with a PR-4000 flow controller governs the 125 SCCM flow of gas into HELIX. The gas pressure is measured with a Balzers PKR250 full range pressure gauge mounted on the vacuum chamber approximately 0.5 m from the closed end of the plasma source chamber, i.e. the pressure measurements are performed at the radial boundary of the plasma. For the measurements reported here, the helium gas was fed into the plasma source from the end, the HELIX magnetic field (B_{H}) was 560 G, the LEIA magnetic field (B_{L}) was zero, the antenna frequency was 13.56 MHz, the rf power was 900 W, and the fill pressure was 18 mTorr. An absolutely calibrated Baratron pressure gauge mounted on the vacuum chamber in the middle of the HELIX chamber was used to calibrate the Balzers gauge measurements of the fill pressure with the rf antenna turned off [21]. For these source parameters, smoothed plots of the typical electron density (n_{e}) and electron temperature (T_{e}), obtained with a rf-compensated Langmuir probe [22], as functions of axial distance from the rf antenna (z) and radial distance (r) are shown in figure 2.

In its first application in plasma, LIF was used to measure the velocity distribution function (VDF) of ions in an argon plasma [23]. Since then, LIF has been used to measure ion, neutral atom, and molecule velocity distributions as well internal magnetic and electric fields. In a typical LIF measurement system, a very narrow bandwidth laser is

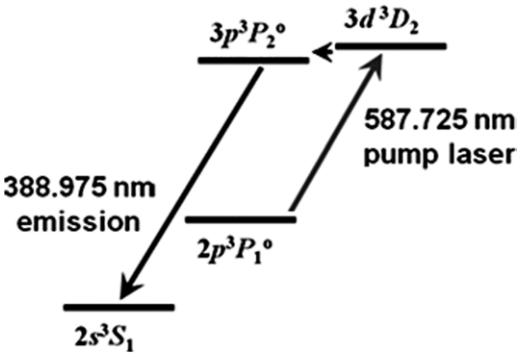

Figure 3. The four-level neutral helium LIF scheme used in these experiments. After being excited to the $3d^3D_2$, state, electrons are knocked into the $3p^3P_2$ state through collisional processes. Wavelengths shown are the vacuum values.

swept over a narrow frequency range while illuminating a collection of particles having a thermally broadened VDF. The illuminated particles absorb a photon and are pumped into an excited state when the laser appears at the appropriate frequency in their respective rest frame. Typically, ions or atoms are considered to have a Maxwellian VDF

$$f(v) \propto \exp\left(-\frac{m(v-v_0)^2}{2k_B T}\right), \qquad (1)$$

where m is the mass, v_0 is the average flow speed of the entire distribution, k_B is Boltzmann's constant, and T is the temperature. For neutral helium LIF measurements, a laser tuned at 587.725 nm (vacuum wavelength) pumps electrons in the $2p^3P_1^o$ state to the $3d^3D_2$ state, where collisions with electrons results in transfer from the $3d^3D_2$ state to the energetically nearby $3p^3P_2^o$ state. The $3p^3P_2^o$ state decays to the $2s^3S_1$ state by emission of 388.975 nm light. The partial Grotrian diagram of figure 3 shows these processes.

The laser system used to excite the initial state consists of a 10 W Spectra-Physics Millennium Pro doubled YAG laser that pumps a Sirah Matisse-DR tunable ring dye laser. Rhodamine-6G dye is used to obtain 1400 mW of laser power at 587.725 nm. A 1% beam splitter directs a portion of the laser output through an iodine cell and into a Bristol Instruments 621-VIS wavelength meter. Fluorescent emission from the iodine cell is recorded for each scan of the laser wavelength as a consistent zero-velocity reference and to compensate for any laser drift [24]. The molecular iodine absorption lines over the range of wavelengths used here are available in the literature with high accuracy [25–27]. The wavemeter also records the absolute laser frequency during each scan. The remaining 99% of the laser output is mechanically chopped at 2 kHz and conveyed to the helicon source laboratory through a multimode, non-polarization preserving optical fiber. The optical fiber is mated to a set of injection lenses mounted at the end of the HELIX chamber and aligned along the magnetic field axis, i.e. parallel injection. While the laser frequency was swept over 20 GHz, the fluorescent emission from the excited state was collected at various axial locations downstream of the rf antenna. The collected light was transported via optical fiber to a filtered, high-gain Hamamatsu photomultiplier tube

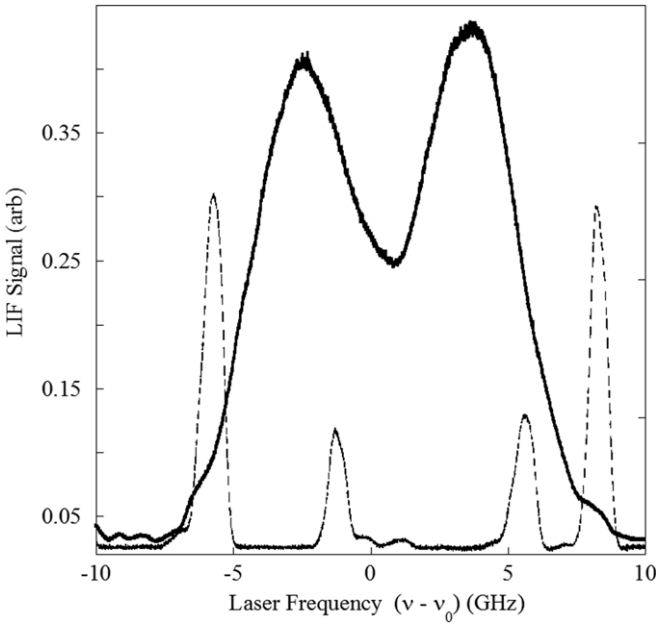

Figure 4. Typical on-axis, parallel neutral helium LIF measurement (solid line) obtained 85 cm downstream of the driving antenna. The simultaneously measured fluorescence spectrum of molecular iodine (dashed line) provides an absolute flow velocity reference.

(PMT). The PMT signal was monitored with a Stanford Research SR830 lock-in amplifier referenced to the laser modulation signal. The injection optic was mounted on a computer controlled Velmex™ stepping motor stage, enabling scanning of the injected light across the plasma radius.

A radially scanning collection optic was constructed specifically for the experiments reported here. It consists of a lens tube in which two plano-convex lenses are positioned to collect maximum light from a volume of 4.18×10^{-3} cm^{-3} at focal length of 37.5 cm. The lens tube slides within a guide tube in 1 mm steps. The guide tube is mounted on a $2\frac{3}{4}$ Conflat™ window. The entire collection assembly mates to one of the four gate valves at axial locations of 55, 70, 85 and 100 cm downstream of the rf antenna. To maintain a fixed light collection volume, the injection optic is moved to the same radial location for each change in position of the focus of the collection optic with a computer-controlled Velmex™ stepping motor assembly. Thus, the distance from the injected laser beam to the collection lens is the same for every radially resolved measurement. With this experimental configuration, both the axial and radial dependences of the LIF signal are obtained.

3. Optical depth measurements of the neutral density

A typical parallel neutral helium VDF measurement obtained at the center of the plasma and 85 cm downstream of the rf antenna is shown in figure 4. The center of the measurement window corresponds to the center of the absorption line, 578.725 nm, and the laser power exiting the injection optical fiber is 40 mW. Surprisingly, the measured VDF appears to be

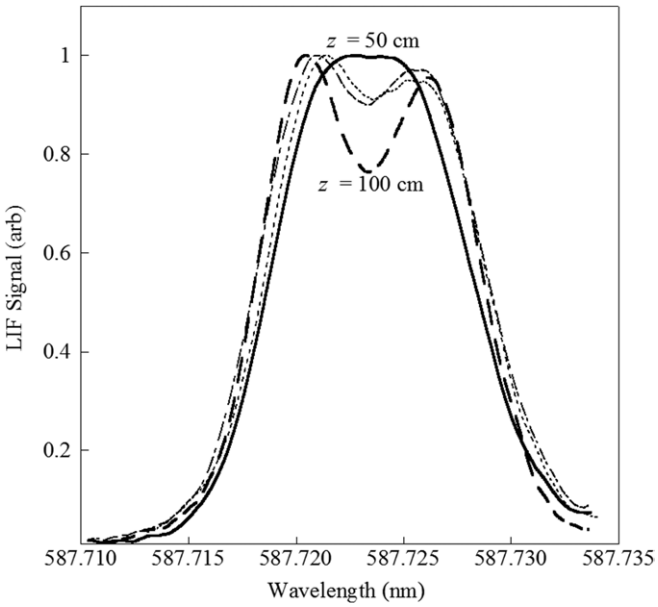

Figure 5. On-axis VDF measurements at axial locations of 55 (solid line), 70, 85 and 100 cm (dashed line) downstream of the driving antenna. The 'dip' in the VDF increases with increasing distance.

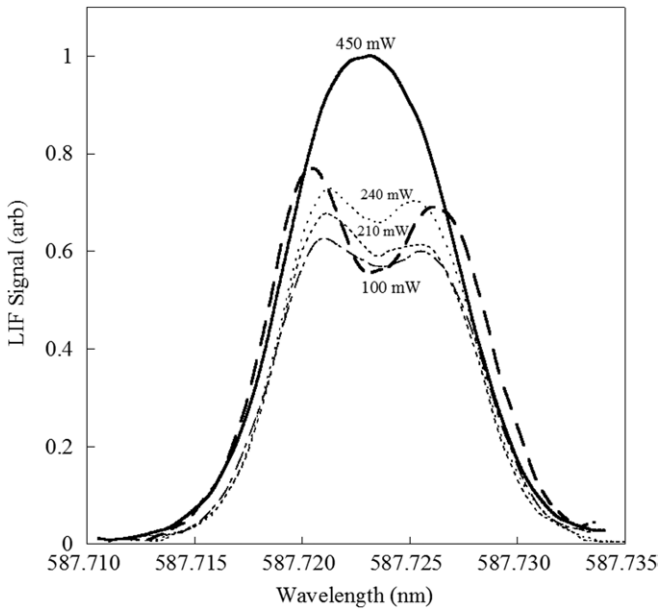

Figure 6. On-axis, parallel neutral helium LIF measurements as a function of injected laser power, 100 cm downstream of the rf antenna. The laser powers, starting from the topmost curve, are 450, 240, 210, 170 (unlabeled) and 100 mW.

bi-modal. Further inspection reveals that the VDF is not bi-modal, but that the middle portion of the VDF is suppressed in the LIF signal at 85 cm downstream because of the strong absorption of the laser light at the peak of the absorption line. As the laser beam travels through the plasma, the $2p^3P_1^o$ metastable state absorbs so much of the laser light at the peak of the VDF that there is not enough laser power to uniformly pump the metastable state at the downstream collection locations.

LIF measurements of the neutral VDF along the plasma axis for different downstream collections distances are shown in figure 5 for an injected laser power of 100 mW. Each measurement is normalized to its maximum value. The relative depth of the signal decrease, the 'dip,' clearly increases with increasing axial distance, a clear signature of an optically thick medium. The slight shift in the center of the VDF to shorter wavelengths indicates a small, but finite, flow of the neutral atoms in the direction along the injected laser beam, i.e. downstream from the antenna. To confirm that the dip in the VDF arises from absorption of the laser light by the neutral gas in the plasma, additional VDF measurements were obtained at different injected laser powers. Shown in figure 6 are LIF VDF measurements obtained at the center of the plasma, at $z = 100$ cm downstream of the driving antenna, and for injected laser powers of 450, 240, 210, 170 and 100 mW. The depth of the dip in the VDF measurement clearly decreases with increasing injected laser power. As the laser power becomes large enough to get through the column of absorbing neutrals in the $2p^3P_1^o$ metastable state, the shape of the VDF approaches that of a Gaussian.

If it were possible to directly measure the laser intensity as a function of axial distance, e.g., by moving a laser power meter along the axis of the experiment, the metastable density could be calculated directly from the decrease in the transmitted laser intensity. In an optically thick medium, the transmitted intensity decreases exponentially

$$I = I_0 e^{-\tau_0} = I_0 e^{-lz}, \tag{2}$$

where l is the absorption scale length and the inverse of the absorption scale length is the optical depth, τ_0. The mean optical depth [28] is given by

$$\tau_0 = \frac{N g_1 A_{21} \lambda_0^3}{8 g_1 \pi^{3/2} v_{th}} D, \tag{3}$$

where D is the characteristic length of the plasma, N is the density of the absorption centers in the medium (the density of the metastable state in this case), $g_1 = g_2 = 3$ are the statistical weights of the lower and upper levels, respectively, $A_{21} = 2.94 \times 10^7\ s^{-1}$ is the tabulated transition probability, λ_0 is the central wavelength of the transition, and v_{th} is the thermal velocity of the helium atoms. All the terms in equation (3) are known except for the metastable density and the thermal speed of the neutrals.

Since it is not possible to directly measure the laser intensity along the axis of the experiment, the relative depth of the 'dip' in the VDF measurement was used to estimate the amount of absorption of laser light along the helicon source axis. The dip itself is fit with a Gaussian function that is then subtracted from a Gaussian 'parent' VDF. A nonlinear fit of the combined model functions to the absorption feature dominated VDF is then used to extract the 'original' amplitude of the VDF. The ratio of the magnitude of the dip to the magnitude of the parent VDF versus axial location decreases exponentially and the decay rate provides an estimate of the mean metastable neutral density along laser path. An example of a reconstructed parent VDF using the nonlinear bi-Gaussian fitting process is shown in figure 7. The thermal velocity of the atoms is estimated from the width of the reconstructed VDF.

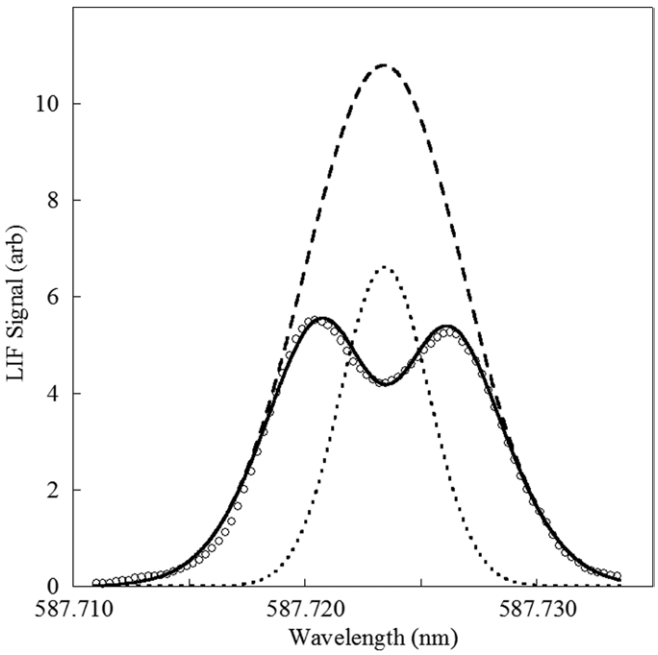

Figure 7. A typical on-axis, LIF measurement of the VDF (open circles) and a nonlinear fit (solid line) of assuming a Maxwellian 'parent' VDF (dashed line) and a Gaussian absorption feature (dotted line). The ratio of the dip's depth (I) to the amplitude of the parent LIF VDF (I_0) is used to determine the neutral density; as explained in the text.

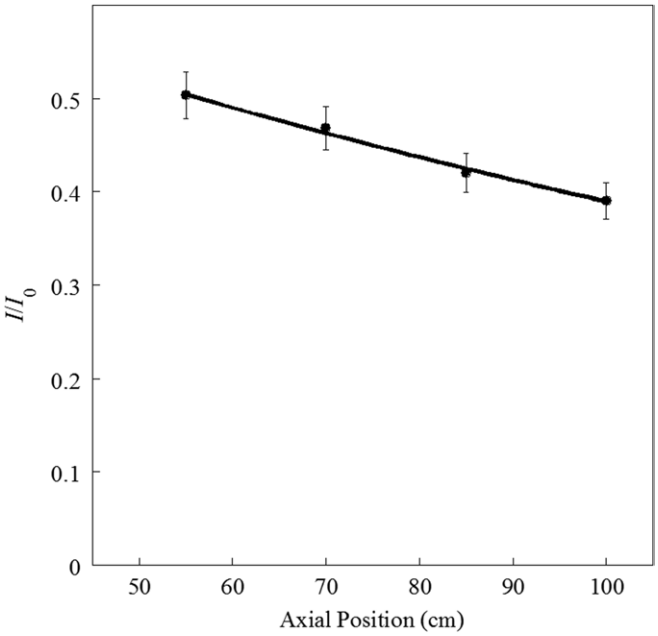

Figure 8. The ratio of the dip at the center of the on-axis VDF measurements, I/I_0, extracted from each normalized VDF plotted versus the four axial distances. Also shown is an exponential fit to the measurements.

Because the same set of collection optics is moved along the axis of the device, the size of the collection volume remains constant throughout the measurement process. To account for any changes in the overall LIF signal strength due to divergence of the injected laser beam or misalignment at each axial location, each VDF measurement was normalized so that the peak of the parent VDF was set to unity. The ratio of the dip depth to the amplitude of the parent VDF, I/I_0, extracted from each normalized VDF, is plotted versus the four axial distances, as shown in figure 8. Also shown in figure 8 is an exponential fit to the absorption measurements. The optical depth obtained from the exponential fit is $l = (5.8 \pm 0.03) \times 10^{-3}$ cm^{-1}. Using the measured neutral temperature of 0.06 eV (from the width of the parent VDF), the measured optical depth corresponds to a metastable density of $(6.6 \pm 0.2) \times 10^9$ cm^{-3}. The metastable density alone, however, does not provide a direct measure of the neutral density along the axis of the plasma source. The expected ground state neutral density, based on the pressure of the background neutral gas, is 6.4×10^{14} cm^{-3}. The dramatic difference in densities simply reflects the fact that the excited metastable state population is a mere fraction of the total neutral density.

Calculation of the total neutral density population from the measured metastable density requires the additional step of performing a CR simulation of the helium plasma. CR models for helium are valid for helium plasmas with electron densities between 10^{10} and 10^{13} cm^{-3}. Unlike LTE models (partial local thermodynamic equilibrium models in which only collisions determine the relative state densities) and CE models (coronal equilibrium models in which radiative processes dominate), a CR model includes both collisional and radiative processes for population and depopulation of the excited states. In a CR model, the density of an excited metastable state p reaches a steady-state value given by

$$n_{z-1}(p) = R_0(p) \cdot n_e \cdot n_z + R_1(p) \cdot n_e \cdot n_{z-1}, \qquad (4)$$

where z is the degree of ionization of the state and$R_0(p)$ and $R_1(p)$ are the electron density and temperature-dependent recombination and ionization coefficients, respectively. For $z = 1$, $n_0(1)$ is the ground state neutral density while $n_0(p)$ is the neutral density of the population excited to the p state. The recombination coefficients for the $2p^3P_1^o$ state (state p in equation (4)) are tabulated in the literature [29].

Using the electron densities and temperatures shown in figure 2, the CR model is run for different ground state neutral densities until the predicted density for the metastable state of the helium LIF sequence equals the values of the absolute density of metastables obtained from the optical depth measurements. This process is then repeated for different sets of plasma source parameters. For example, the metastable density of $(6.6 \pm 0.2) \times 10^9$ cm^{-3} is predicted by the CR model to occur for our measured electron densities and temperatures with an on-axis ground state neutral density of 4.4×10^{12} cm^{-3}. This value of neutral density is significantly smaller than the estimated edge neutral density of 6.4×10^{14} cm^{-3} and comparable in magnitude to the measured on-axis plasma density of 6.3×10^{12} cm^{-3} (see figure 2). Taking the ratio of the measured on-axis plasma density to the sum of the calculated on-axis neutral density plus the plasma density yields a plasma ionization fraction of 58% at $r = 0$; as well as a decrease of the neutral density from the edge to the center of the plasma of over 90%. Such a level of ionization is consistent with expectations for a plasma with an electron temperature between 5 and 10 eV.

The substantial decrease in neutral density from the location of the pressure gauge to the axis of the plasma likely results from the strong gradient in neutral pressure along the axis of the helicon source, due to the large pumping rate in the LEIA chamber, ionization, and neutral pumping [5, 6] in the discharge.

4. Comparison of static and actively pumped discharges

Traditionally, laboratory plasma sources are operated with active gas injection and pumping during the experiment. The flowing gas helps one to cool plasma generation mechanisms, e.g. filaments, capacitive plates, etc and reduces the buildup of impurities that might desorb from the chamber walls or other internal surfaces. Continuous gas exchange, however, does remove energy from the discharge through the loss of long-lived metastable neutral and ion states as well as classical thermal convection. Using the capability to non-invasively measure the mean neutral density along the axis of the HELIX source, we have examined the conventional wisdom regarding the benefits of flowing versus static, no pumping discharges. Two cases are considered (1) a constant pressure flowing gas discharge in which the helium gas was actively injected into the chamber and pumped away at both ends while maintaining a steady-state pressure of 18 mTorr and (2) a static discharge in which the chamber was filled and then sealed at the same steady-state neutral pressure. In both cases, the neutral pressure measured at the wall of the chamber at one end of the source was held fixed at 18 mTorr; which yields as edge neutral density of 6.4×10^{14} cm^{-3} assuming room temperature neutrals.

Shown in figure 9 is a comparison of the radial profiles of electron density and temperature, as measured with an rf-compensated Langmuir probe, 55 cm downstream of the driving antenna for both cases. The measurements indicate that the on-axis plasma density increases by 42% and that the average plasma density (averaged over all radii) increases by 38% in the static discharge case. For the same plasmas, the on-axis electron temperature decreases by 14% and the electron temperature averaged over all radii decreases by 15%. Consistent with the increase in plasma density, the optical depth at the center of the plasma decreases in static discharges, i.e. the ionization fraction in the center of the discharge appears to increase. For the two gas flow cases, the parallel VDF measurements obtained at $z = 100$ cm and $r = 0$ cm are shown in figure 10. The same injected laser power was used for both measurements and the absorption, i.e. the neutral helium metastable density, is clearly reduced in the static case.

The LIF VDF measurements were repeated over a radial range 0 to 1.1 cm with one millimeter resolution for all four axial locations: 55, 70, 85 and 100 cm, and for both fueling configurations. To keep the gain of the LIF detector constant for all the measurements and to ensure that sufficient neutral helium metastables were available to absorb a measurable fraction of the laser light (the population of the metastable state depends strongly on the electron density and electron temperature), the radial span was limited to just a little more than one centimeter. For each VDF measurement, the parent VDF was reconstructed and then the I/I_0 ratios were calculated for each axial position at each radial location. The nonlinear fits used to construct the parent VDFs were required to yield physically reasonable neutral helium temperatures, ~0.05 eV [21]. The optical depth at each radial location was again determined through exponential fits to the absorption data. The calculated metastable density was related to the ground state density of neutral helium through runs of the CR

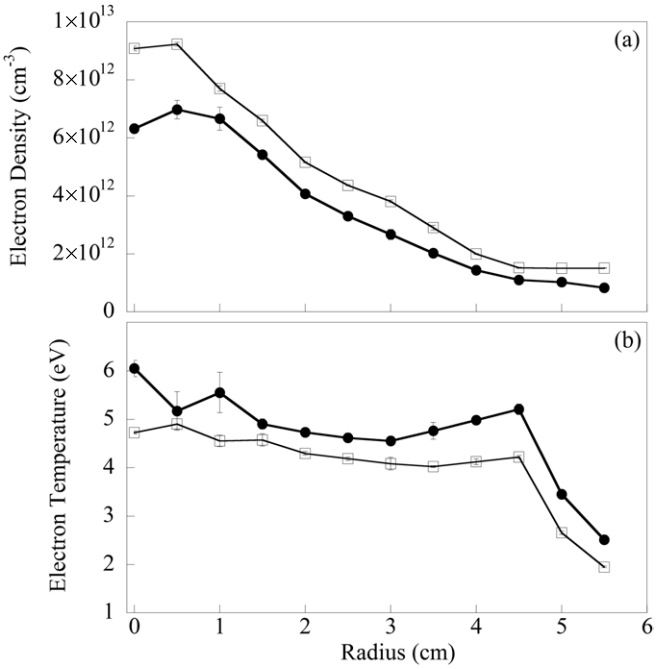

Figure 9. (*a*) Electron density versus radius for the flowing gas with active pumping (filled circles) and static (open squares) discharges at 18 mTorr. (*b*) Electron temperature versus radial location for the same two cases.

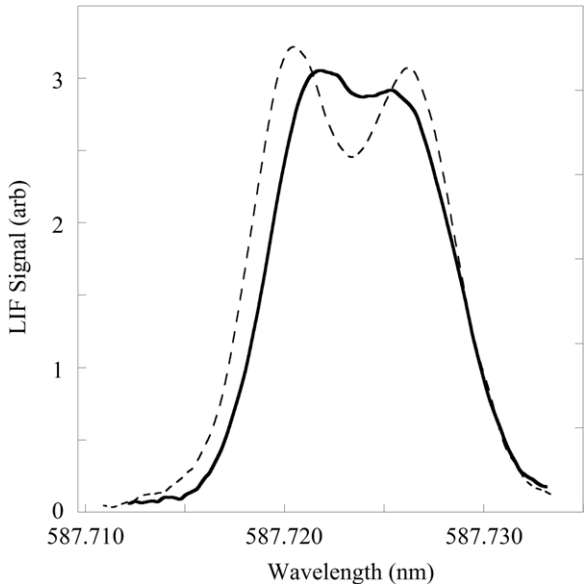

Figure 10. On-axis, parallel neutral helium LIF measurement for a static (solid line) and flowing (dashed line) discharge. The same laser power was used for both measurements at $z = 100$ cm.

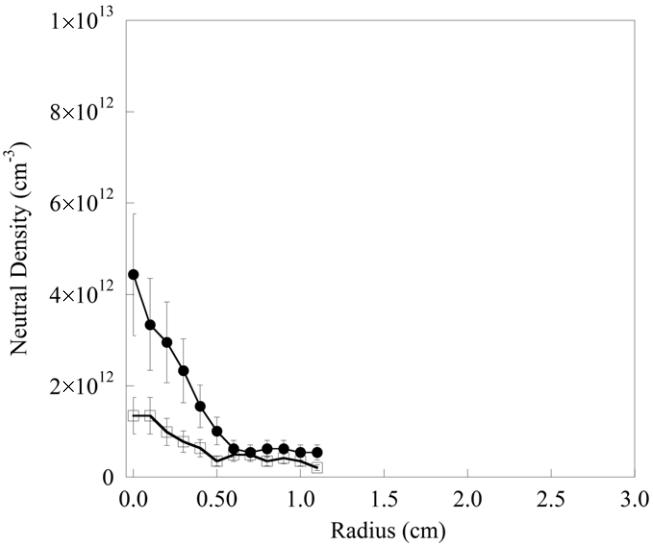

Figure 11. Neutral density versus radial location for two different fueling configurations, flowing gas with active pumping (filled circles) and 'static,' no pumping (open squares).

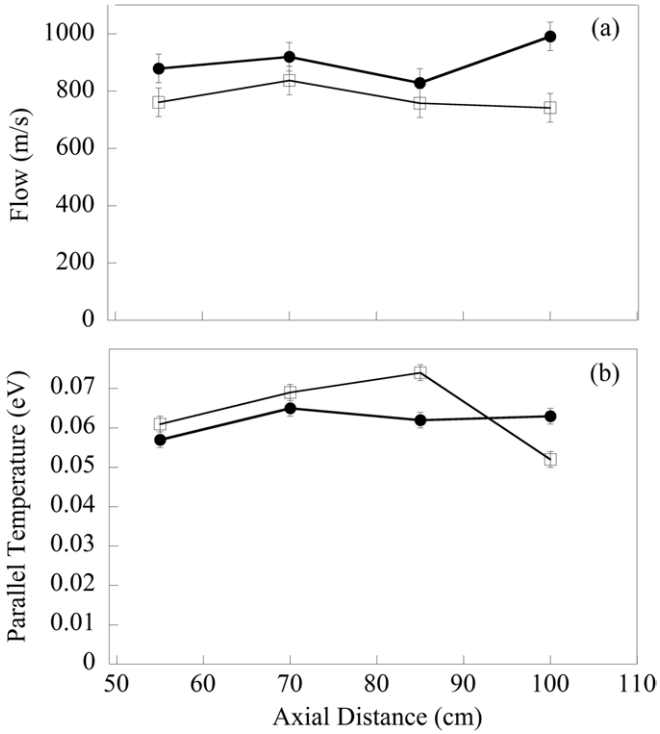

Figure 12. (*a*) Parallel, on-axis neutral velocity versus distance along the axis of the source for the flowing gas (filled circles) and static (open squares) fueling configurations. (*b*) The parallel neutral temperatures for the same fueling cases.

model which included the variations in electron density and temperature at each radial location.

Figure 11 shows the comparison of the calculated profiles of the ground state neutral density for the two cases. The average (over 1 cm) neutral density decreases 55% in the static fueling case. The calculated on-axis neutral density of 1.4×10^{12} cm^{-3} for the static case is a 70% decrease compared with the flowing case. More importantly, the helium ionization fraction jumps from roughly 50% in the flowing case to nearly 90% in the static fueling case. Note that in the flowing gas case, there is a distinct peak in the calculated ground state neutral density profile on axis. Overall, the calculated on-axis neutral densities are two orders of magnitude smaller than the edge neutral pressures deduced from pressure gauge readings. Note also that these measurements only extend over the very central portion of the plasma; thus the much larger neutral pressures at the chamber boundary are not evident in figure 11, i.e. there is a substantial decrease in the neutral density from the plasma edge to the axis of the plasma in both cases. However, in the static fueling case, the calculated neutral densities are even smaller and the neutral density profile is flatter. That the decrease in the magnitude of the neutral density obtained from the LIF measurements plus the CR model calculation is equal to and opposite in sign to the change in the measured plasma density (2×10^{12} cm^{-3}) provides additional confirmation that the use of the CR model to estimate the ground state neutral density from the measurements of the metastable density measurement yields reasonable values.

The modest peak (at $r = 0$) in the calculated ground state neutral density profile for the both cases (flowing and static gas discharges) is a result of the measured hollow electron density profile. As shown in figure 9, the electron density is peaked at $r =\sim 5$ mm, not the center of the discharge. Because the zero-dimensional CR model does not fully account for geometrical effects such as radial transport that can dominate the relative state populations in the center of the discharge, nor does it include possible effects of non-Maxwellian electron distribution functions that might exist along the axis of a helicon source, it is possible that the structure near the axis in the calculated ground state neutral density profile reflects an incomplete accounting for transport or superthermal electrons. However, the change in the CR model calculated neutral density is consistent in both sign and magnitude with the change in the measured plasma density. Thus, if the radial neutral density profile predicted by the CR model, particularly the on-axis peak, is not representative of the actual neutral density profile, any substitute explanation must also reproduce the measured change in on-axis plasma density between the static and flowing cases.

The reconstructed parent VDFs also provide a measure of the bulk flow and the parallel temperature of the neutral helium at each measurement location. In contrast to the absorption measurements which are line integrated over the path length of the laser beam in the plasma, the flow and temperature measurements are localized to the collection volume of the LIF signal. The measured parallel velocities and temperatures of the neutral helium as a function of axial distance from the driving antenna are shown in figure 12 for both fueling cases at $r = 0$ cm. For the flowing gas case, the parallel neutral helium velocity is directed away from the antenna and increases gradually with increasing distance from the driving antenna. The magnitude of the flow is comparable to the thermal velocity of the neutrals. In the static gas case, the measured parallel flow is uniform along the axis and is again comparable in magnitude to the neutral thermal speed. The

flow speeds in the static case are systematically $100\,\mathrm{m\,s^{-1}}$ slower than when the gas is actively pumped.

For the static fueling case, there is a significant spatial variation in the parallel ion temperature along the source axis. From 55 to 85 cm, the parallel ion temperature increases by roughly 15%. In the flowing gas case, the parallel ion temperature is uniform along the source axis and systematically lower than in the static case.

5. Summary

In this work, we have shown that the line-integrated metastable state density of neutral helium in a helicon source is sufficient to absorb a measurable fraction of an injected laser beam tuned to 587.725 nm. From the measured metastable state densities, the ground state neutral density is calculable with a collisional–radiative model and Langmuir probe measurements of electron density and temperature. In normal operation, the ionization fraction in the helium helicon plasmas ranges from 10% to 50%. When the source is operated in a static fill mode the ionization fraction increases to as much as 90%. In both standard and static modes of operation, the on-axis neutral density is considerably smaller than what would be naively predicted based on pressure gauge measurements at the chamber wall. The overall number density is conserved, with the measurements indicating that the decrease in neutral density results in an equal in magnitude increase in the plasma density. The total thermal pressure at the center of the discharge ($P = n_e kT_e + n_i kT_i + n_o kT_o \sim 50\,\mathrm{mTorr}$) is dominated by the electron pressure and is larger than the measured edge neutral pressure of 18 mTorr. Thus, the remaining radial pressure balance must be provided by the magnetic pressure.

For experiments which require minimal ion–neutral and electron–neutral collisions and large plasma densities, such as Alfvén wave propagation studies, the static mode of operation has obvious advantages. The measured parallel neutral flow is comparable to the neutral thermal speed and the axial gradient in parallel neutral flow speed vanishes in the static mode of operation; consistent with the lack of an axial neutral pressure gradient in the static case. A modest level of neutral heating occurs downstream of the driving antenna in the static mode of operation.

Acknowledgments

This work was supported by NSF Award No PHY-0611571. The authors wish to thank Professor Fred Skiff for his advice on the analysis of the LIF measurements and Dr Ella Sciamma for use of her CR model code.

References

[1] Okamato A, Hara H, Nagaoka K, Yoshimura S, Vranješ J, Kono M and Tanaka My 2003 *Phys. Plasmas* **10** 2211
[2] Watts C and Hanna J 2004 *Phys. Plasmas* **11** 1358
[3] Houshmandyar S and Scime E 2011 *Phys. Plasmas* **18** 112111
[4] Woods L C 1962 *J. Fluid Mech.* **13** 570
[5] Keesee A M and Scime E E 2006 *Rev. Sci. Instrum.* **77** 10F304
[6] Gilland J, Breun R and Hershkowitz N 1998 *Plasma Sources Sci. Technol.* **7** 416
[7] Sciamma E M, Begtson R D, Rowan W L, Keesee A M, Lee C A, Berisford D, Lee K and Gentle K W 2008 *Rev. Sci. Instrum.* **79** 10E324
[8] Aanesland A, Liard L, Leray G, Jolly J and Chabert P 2007 *Appl. Phys. Lett.* **91** 121502
[9] Denning C M, Wiebold M and Sharer J E 2008 *Phys. Plasmas* **15** 072115
[10] Shimada M, Tynan G R and Cattolica R 2007 *Plasma Sources Sci. Technol.* **16** 193
[11] Cho S 1999 *Phys. Plasmas* **6** 359
[12] Fruchtman A, Makrinich G, Chabert P and Rax J-M 2005 *Phys. Rev. Lett.* **95** 115002
[13] Raimbault J-L, Liard L, Rax J-M, Chabert P, Fruchtman A and Makrinich G 2007 *Phys. Plasmas* **14** 013503
[14] Fruchtman A, Makrinich G, Raimbault J-L, Liard L, Rax J-M and Chabert P 2008 *Phys. Plasmas* **15** 057102
[15] Hartig M J and Kushner M J 1993 *Appl. Phys. Lett.* **62** 1594
[16] Kilgor M D, Wu H M and Graves D B 1994 *J. Vac. Sci. Technol.* B **12** 494
[17] Shimada M, Tynan G R and Cattolica R 2008 *J. Appl. Phys.* **103** 033304
[18] O'Connell D, Gans T, Crintea D L, Czarnetzki U and Sadeghi N 2008 *Plasma Sources Sci. Technol.* **17** 024022
[19] Houshmandyar S, Sears S, Chakraborty Thakur S, Carr J Jr, Galante M and Scime E 2010 *Rev. Sci. Instrum.* **81** 10D704
[20] Kline J L, Scime E E, Boivin R F, Keesee A M and Sun X 2002 *Plasma Sources Sci. Technol.* **11** 413
[21] Hardin R A 2008 *PhD Dissertation* West Virginia University Morgantown, WV
[22] Keiter P A, Scime E E and Balkey M M 1997 *Phys. Plasmas* **4** 2741
[23] Stern R A and Johnson III A 1975 *Phys. Rev. Lett.* **34** 1548
[24] Scime E, Hardin R A, Biloiu C, Keesee A M and Sun X 2007 *Phys. Plasmas* **14** 043505
[25] Gerstenkorn S and Luc P 1979 *Rev. Phys. Appl.* **14** 791
[26] Gerstenkorn S and Luc P 1980 Atlas du spectre d'abrorption de la molecule de l'iodine entre 14800-20000 $\mathrm{cm^{-1}}$, edition du CNRS vol 15
[27] Salami H and Ross A J 2005 *J. Mol. Spect.* **233** 157
[28] Boivin R F, Kline J L and Scime E E 2001 *Phys. Plasmas* **8** 5303
[29] Sciamma E M 2007 *PhD Dissertation* University of Texas-Austin, Austin, TX